Parametric Aeroelastic Analysis of Composite Wing-Boxes with Active Strain-Energy Tuning

F. Persiani, Dip. Costr. Mecc. Aeron. Nuclear, Università Bologna
P. Santini, Dipartimento Aerospaziale, Università "La Sapienza" Roma
G.M. Saggiani, Dipartimento Aerospaziale, Università "La Sapienza" Roma

ABSTRACT

The general equations for the static aeroelastic behaviour of a general planform wing, with an adaptive structural box in composite material containing strain controlled fibers, are written. Upper skin and lower skin fibers can be controlled independently, giving both in plane and bending strains. The expressions for strain-energy associated with in plane active stresses and with bending stresses respectively are computed, by using a set of describing functions; for each of them a modal amplitude is defined and it is ranked among the unknowns. Thus a set of non-linear finite equations is obtained. For practical applications, the maximum value of the active forces is prescribed and there results a set of algebraic equations, from which the structural response can be computed.

Numerical examples show the effect of the activation upon structural deformations and upon total aerodynamic forces.

1. Introduction

Materials capable of an active control via the variation of a physical parameter (temperature, applied electric potential) can be incorporated in the body of composite materials as actuators, in such a way as to produce controlled and reversible deformations of structural elements. Association of such actuators with sensors incorporated in the material leads to the concept of "Smart Structures", capable of adapt themselves and respond to different operational conditions [1][2][3].

Several applications are possible: e.g., plate-like structures can be deformed in bending, twist and in-plane-stresses without exchanging forces with the external environment, and without experiencing inertia forces. It is thus possible to control static and dynamic deformations of aerospace structures: as an example, by employing induced deformation actuators incorporated in the element of a lifting surface, it is possible to control its aeroelastic behaviour [4].

Deformation control devices include (i) piezo effects [5] (ii) shape memory alloys [6] (iii) electro strictors (iv) magneto strictors (v) thermal expansion, etc. Among them, (i) and (ii) are the most widely used for structural applications; piezo on account of the easiness of adjustment and response, shape memory alloys on account of their capability of inducing high stress levels.

Major drawbacks are associated with the limitation of stress,(and, therefore, of the total excursions) for the former, and with the comparatively slow deformation velocity (very low bandwidth) and with difficulties in controlling temperatures for the latter.

In this paper, attention is focused on the analysis of a lifting surface, whose structure may be considered to consist of one or more boxes in composite, having various layers, some of them with control induced deformations. Planform of the surface can be allowed to consist of several trapezoids (differently than in some simple cases of the current literature), and, also, skin thickness is allowed to vary along the wing.

A computing technique, based on Gyles' model [7] is presented in such a way as to account for several activating policies. The model is relatively simple, and it allows to use reasonably compact symbolic expressions. It is thus possible to have a better understanding of the effects associated with the variation of parameters defining structure geometry and material properties.

2. Definition of parameters and unknowns

The structure of the wing box is represented through an equivalent plate, following Gyles' approach, here suitably modified in order to account for active elements (shape-memory alloys).

The wing model consists of two "skins" (or faces) symmetric with respect to the mean surface: it is also assumed that the core is consisting of

weightless webs, having infinite in-plate-stiffness and zero out-of-plane stiffness (Fig 1).

Each of the two skins consists of L_1 laminae; note that L_1 is allowed to vary with the spanwise coordinate y, Fig. 2. Therefore the total thickness of the skin is given by:

$$t = t(y) = L_1(y)\, t_S \tag{1}$$

where t_S is the thickness of a lamina.

A "lamina" consists of L_2 sheets (or plies), each having thickness t_p, so the total thickness of a lamina is given by:

$$t_S = L_2 t_p \tag{2}$$

In the following we shall regard L_1 as a continuous function of y, although, as a matter of fact, it is not continuous. Such approximation is justified if $t << h$ and $t_S << t$, where $h = h(y)$ is the height of the wing box (Fig 1). The elastic properties of the laminae and of the sheets are defined in Appendix I .

For the definition of the wing planform, we need a system of rectangular coordinates (x,y), Fig. 2. We define shape (or modal) functions $F_{ij}(x,y)$, of amplitude q_{ij}. In the general case q_{ij} are functions time t; as a matter of fact, in this paper, we consider only static problems, so q_{ij} is independent of t. Therefore we may write the elastic displacement of the plate under the form:

$$W(x,y) = \Sigma_i \Sigma_j q_{ij} F_{ij}(x,y), \qquad i=0,...,M_1 \ ; \ j=2,...,M_2 \tag{3}$$

where the describing functions are taken as:

$$F_{ij}(x,y) = (x^i y^j)/b^{i+j} \tag{4}$$

and b is the wing-semispan, Fig.2..

The reason for starting with j=2 in the Eq.(3) is in the need to cope with root conditions.

3 The modified equivalent plate

For further developments, as said, we shall use Gyles' model, applying the principle of virtual work. For this purpose we must express (i) the strain-energy of the structure, (ii) the work done by the external forces and (iii) the potential energy associated with fibers activation. Obviously we do not calculate kinetic energy, since we are considering static cases only.

For (i) we have the surface density of the strain energy expressed by

$$\Pi e = (D_{11}\, W^2_{,xx} + 2\, D_{12}\, W_{,xx} W_{,yy} + D_{22}\, W^2_{,yy} + 4\, D_{16}\, W_{,xx} W_{,yy} + 4\, D_{26}\, W_{,yy} W_{,yy} + 4\, D_{66}\, W^2_{,yy}) / 2 \tag{5}$$

where D_{ij} are the constants of each skin, defined in Appendix II, and subscript preceded by a comma denotes differentiation with respect to the relevant variable.

For (ii) we have the work of the external loads p=p(x,y) per unit area:

$$L_s = p\, W \tag{6}$$

As far as (iii) is concerned, let P_{au} denote the number of active elements in the upper skin; so the in-plane total active forces (per unit length) are given by:

$$N_u = \Sigma_k\, [\sigma_u{}^*_x, \sigma_u{}^*_y, \sigma_u{}^*_{xy}]_k\, t_S, \qquad k = 1,...,P_{au} \tag{7}$$

where the $\sigma_u{}^*$'s denote the control stresses induced in active layers. By the same token we may define the total active forces in the lower skin:

$$N_l = \Sigma_k\, [\sigma_l{}^*_x, \sigma_l{}^*_y, \sigma_l{}^*_{xy}]_k\, t_S, \qquad k = 1,...,P_{au} \tag{8}$$

We shall consider, in the following, symmetric shells only; so we can split (7) and (8) into a symmetric (or membrane) component:

$$N_0 = (N_u + N_l)/2 \quad (9)$$

and an antisymmetric (or flexural) component:

$$N_1 = (N_u - N_l)/2 \quad (10)$$

which causes a bending moment $N_1 h$.

The work per unit area associated with the membrane component N_0 is given by:

$$P_{N0} = N_{0x} W^2_{,x} + 2 N_{0xy} W_{,x} W_{,y} + N_{0y} W^2_{,y} \quad (11)$$

and the work associated with the flexural component N_1:

$$\Pi_{N1} = 1/2\ h\ (N_{1x} W_{,xx} + 2 N_{1xy} W_{,xy} + N_{1y} W_{,yy}) \quad (12)$$

Let the activation level be defined through parameters Ψ_0 and Ψ_1, equal to the ratio of current values to maximum values:

$$N_0 = \Psi_0 N_{0max}$$
$$N_1 = \Psi_1 N_{1max} \quad (13)$$

The generation of the control forces is discussed in Appendix III.

Thus, by using the principle of virtual work, we obtain the solving equation for the structural response as:

$$(\mathbf{K}_0 + \Delta\mathbf{K}_e + \mathbf{K}_{N0}\,\Psi_0)\,\mathbf{q} = \mathbf{R}_{N1}\,\Psi_1 + \mathbf{Q} \quad (14)$$

In eq. (14):
- $\mathbf{K}_0$ is the stiffness matrix for the whole structure, as calculated from the modes (4);
- $\Delta\mathbf{K}_0$ is the change in $\mathbf{K}_0$ due to the change in the modulus of elasticity of the active fibers (we shall neglect it in the subsequent numerical developments);
- $\mathbf{K}_{N0}$ is the matrix associated with the work done by N_0;
- $\mathbf{R}_{N1}$ is a vector associated with the work done by N_1;
- $\mathbf{Q}$ is the vector of external forces.

We note that each term in (14) is obtained by writing Lagrange functionals upon integration of the relevant expressions per unit area, (i) (5) (11) (12) over the planform area occupied by the structural box and (ii) (6) over the area of the lifting surface, which is in general wider. The expression of $\mathbf{K}_{N0}$ and $\mathbf{R}_{N1}$ are given in Appendix II.

4. Aerodynamic forces

At this point we introduce aerodynamic forces into the term $\mathbf{Q}$. For this purpose we must write the well known integral equation of the lifting surface theory:

$$w(x,y)/U_0 = (1/(8\pi)) \oint\!\!\!\!\!\!- _{\Sigma} C(x_0,y_0)\,K(x,y,x_0,y_0)\,dxdy \quad (15)$$

where Σ is the wing surface, and the kernel is given by

$$K(x,y,x_0,y_0) = \{(1+(x-x_0)/\sqrt{[(x-x_0)^2+\beta^2(y-y_0)^2]}\}/\,(y-y_0)^2 \quad (16)$$

Furthermore, U_0 is the free stream speed, β is Prandtl-Glauert parameter, $\oint\!\!\!\!\!\!-$ denotes the principal part of an integral, $w(x,y)$ is the downwash at (x,y) and $C = C(x,y)$ is the local pressure coefficient. As well known, an approximate expression for C is

$$C(x,y) = 1/c(y)\ \sqrt{[(1-u)/u]}\ \Sigma_n \Sigma_m u^n\, B_{mn} \sin[(2m+1)\,\theta] \quad (17)$$
$$m=0,...,m' \ ; \quad n=0,...,n'$$

where u and η are defined in Fig.3, and $\theta = \cos^{-1}(\eta)$, according to Multhopp's well known rule. The integers m',n' are chosen on the basis of the required accuracy. The constants B_{mn} are the unknowns of the aerodynamic problem, and can be ordered into a single vector $\mathbf{B}$.

A collocation method is used, consisting in imposing tangency condition at $m^* = (m'+1)(n'+1)$ control points on the wing area. The wing planform is divided into m" n" panels; in each panel C is considered constant. For computational efficiency:

$$m'' n'' >> m^*$$

Relevant singularities are duly treated. The numerical computing technique is straightforward [8] and it is not recalled here. Suffice to say that, at the end, a set of linear algebraic equations is obtained

$$\mathbf{A}\,\mathbf{B} = \mathbf{J} \qquad (18)$$

where **J** is the vector of the angles of attack at the control points. Thus, if J_{0r} is the given (or imposed) angle of attack at the r-th control point, we shall have

$$J_r = J_{0r} - 1/U_0\,(\partial W/\partial x)_r \quad ; \; r=1,...,m^* \qquad (19)$$

or

$$J_r = J_{0r} - (1/U_0)\,\Sigma_{ij}\, q_{ij}\,(\partial F_{ij}/\partial x)_r \quad ; \quad \begin{matrix} r=1,...,m^* \\ i=0,..,M_1 \\ j=0,...,M_2 \end{matrix} \qquad (20)$$

If we condense the subscripts (i,j) into a single index s ,as described in Appendix I, and we introduce the matrix $\mathbf{J}_q$ whose elements are given by $[1/U_0\,(\partial F_s/\partial x)_r]$, we can solve Eq.(18) for **B**, obtaining:

$$\mathbf{B} = \mathbf{A}^{-1}(\mathbf{J}_0 - \mathbf{J}_q\,\mathbf{q}) \qquad (21)$$

At this point, in order to compute the generalized aerodynamic forces we use the formula:

$$\mathbf{F}_a = (\partial/\partial\mathbf{q})\,(p_d \int_\Sigma C_p(x,y)\, w(x,y)\, d\Sigma) \qquad (22)$$

where p_d = dynamic pressure. It is very simple to obtain the final expression:

$$\mathbf{F}_a = p_d(\mathbf{R}_0 + \mathbf{R}_q\,\mathbf{q}) \qquad (23)$$

The coefficients of the aerodynamic matrix $\mathbf{R}_q$ and of the vector $\mathbf{R}_0$ are given in Appendix IV.

The solving equation (14) can thus be explicated in the following way, assuming that the only external forces **Q** are the aerodynamic loads $\mathbf{F}_a$:

$$(\mathbf{K}_0 + \Delta\mathbf{K}_a + \mathbf{K}_{N0}\Psi_0 - p_d\mathbf{R}_q)\mathbf{q} = \mathbf{R}_{N1}\Psi_1 + p_d\,\mathbf{R}_0 \qquad (24)$$

5. Method of solution

In general, the problem is well posed if one ranks Ψ_0, Ψ_1, **q** among the unknowns. In this case, one must specify further conditions, e.g., control of angle of attack, or of total lift.

Here we present another approach, consisting in a parametric study of Eq. (24), where Ψ_0, Ψ_1 are given, and the values of **q**, together with the other relevant quantities, are deduced [9]. For this purpose, symbolic calculus, despite its inherent limitations, has proven quite successful. This means solving Eq. (22) as an analytical expression involving Ψ_0, Ψ_1 and p_d, and providing all other useful quantities. Another parametric variable which may be of interest is the imposed angle of attack, included in term $\mathbf{R}_0$.

In the following, numerical developments, the values M_1=2 and M_2=4 were taken; they correspond to a parabolic chordwise variation and to a fourth order spanwise variation of W(x,y). Therefore the order of the system (24) is 9.

6. Numerical example

We consider the untapered wing illustrated in Fig. 4, having the following geometry:

- wing surface	112 m^2
- aspect ratio	9.1

- wing chord 3.5 m
- shell height at root 0.525 m
- shell height at tip 0.350 m

Shell height is linearly varying along the wing span.

The sheets have the following characteristics (see App. I):

E_{11} = 181000 MPa
E_{12} =E_{21} = 2900 MPa
E_{22} = 10300 MPa
E_{66} = 7170 MPa

As far as the structure is concerned, let us define laminae. Each of the laminae consists of 12 sheets; the six external ones are made of carbon fiber composite (CFC), and the six internal sheets are made of NiTiNOL; the latter are the active elements. Tab. I defines the angles of the various sheets with respect to the longitudinal axis of the aircraft to which the structure is supposed to belong.

TAB I

	outer sheets	internal sheets
1	45° + α	α +α_1
2	135° + α	α +α_1
3	90° + α	α +α_1
4	90° + α	α -α_1
5	90° + α	α -α_1
6	90° + α	α -α_1

Here α is the angle of which we may rotate rigidly the lamina for tailoring purposes. Each sheet has a thickness of 0.1 mm.: each skin consists of 23 laminae at the wing root and 12 at the wing tip.

A first investigation was conducted on a simplified model (M_1=2, M_2=3) in order to determine which angle α could give the best wing stiffness , for three angles of sweep. It has also been checked which value of α_1 could give the maximum angle of twist by activating the fibers.

The following results were obtained:

TAB II

angle of sweep	α	α_1
-30°	19°	19°
0°	-26°	30°
30°	-19°	-12°

Fiber activation was considered as described in App. III, with σ_r*max = 500 MPa, and V_α = 0.5. Furthermore, flight conditions of U_0 = 0.75 at the altitude of 25000 ft, were considered corresponding to p_d = 14700 Nm^{-2}.

Some results are presented in the following illustrations. Note that, in order to give a better engineering feeling of the results, the absolute values of the activating uniform σ_r*, as defined in App. III, and not the dimensionless values defined by(13) are used; they are still denoted by Ψ=Ψ_0 = Ψ_1.

Fig. 5 provides the elastic displacement w along the leading edge for different levels of fibers activation in an unswept wing (Λ=0). The effect of reduction of the wing deformation by activating fibers is very clear.

A similar diagram is represented in Fig. 6, giving the chordwise distribution of w for the tip section, where it is seen that not only displacements, but also slope (which is by far the most important quantity from an aerodynamic standpoint) is controlled through activation.

A better understanding of the stabilizing effect of activation is gained by looking at Fig. 7, where two significant parameter are plotted vs. activating intensity: (i)tip-chord leading and (ii)trailing edge respectively.

In Fig. 8 the torsional deformation of the wing is represented as a function of the distance along leading edge (equivalent to a spanwise coordinate). A conclusion that can be drawn, is that at height values of Ψ, the increase in

stabilizing effects with increasing Ψ is rather slow. Equivalent results are given in Fig 9. From a design viewpoint, lift distribution along the wing is of paramount importance,

Fig 10 provides the lift distribution vs. non dimensional spanwise coordinate η ($0 \leq \eta \leq 1$). The shape of the curves is similar and it was also obtained by other authors [10] for the non active case. Again activation reduces load. The results are summarized in Fig. 11 providing the lift slope coefficient k vs. activation.

Fig. 12 illustrates the effect of activation upon the moment coefficient; note that here the moment is taken with respect to the leading edge point of the root section of the wing., S (Fig. 3). In Fig. 12 the values of dC_M/d(angle of attack) , and in Fig 13 the values of dC_L/dC_M are given again vs. activation.

Similar results are plotted in Figs. 14 through 22 for the 30° sweptback wing, and in Figs. 23 to 31 for the 30° sweptforward wing. In comparing the results, however, one must consider that the structure is not the same for the three cases, since the angle α and α_1 are varying according as described in Tab I, II. Detailed comparison of the various results would be too lengthy and beyond the scope of this paper. We can only say that ,f.i., the results prove the capability of the chosen structure and of the activation to control inherently unstable wings such as, f.i., a sweptforward wing.

7. Conclusions

Analysis of a plate-like wing has been conducted in aeroelastic steady conditions, with active fibers providing controls. Amplitudes of degrees of freedom and activation parameters are the quantities of major interest entering the frame of the problem. The resulting governing equations can be solved parametrically by using, f.i., symbolic computer programs yielding analytical (although very complicated) expressions for the unknowns (modal amplitudes). Numerical results carried out for several wing geometry's and activation parameters have shown the adequacy of the method proposed in the paper to serve as a useful tool in the design of active control smart structures systems.

8. Acknowledgments

The Authors are wishing to thank ISAERS, Forli`, Italia, for providing help and support , both in personnel and in computing facilities, in the preparation of the programs and of the numerical examples shown in the paper.

The Authors are also greatly indebted to Paolo Gasbarri for the help received during the preparation of the present paper and for the scientific discussions concerning some specific aspects of the subjects treated above.

APPENDIX I

In Art. 2 we have introduced the concepts of "sheet", "lamina", "skin"'. A sheet is an orthotropic element of composite with one-directional filaments, so its constitutive matrix will have the form:

$$\mathbf{E}_s = \begin{vmatrix} E_{11} & E_{12} & 0 \\ E_{21} & E_{22} & 0 \\ 0 & 0 & E_{66} \end{vmatrix}$$

defined by a set of four parameters.

A lamina will consist of L_2 sheets each at different angle with respect to one of them taken as reference. Finally, the skin will consist of L_1 superposed laminae joint together..

As a conclusion each of the skins can be considered as a single laminate, consisting of $L=L_1*L_2$ sheets, each defined by the above matrix and by an angle α_j. Well known rules [11] allow to pass from the intrinsic reference to the fixed reference for each of them, thus obtaining a matrix $\mathbf{E}_j$. Furthermore we define the thickness t_j and the distance d_j from the mean surface.

So we may write the total stiffness matrix as:

$$\mathbf{D} = \sum_j (\mathbf{E}_j)\, t_j\, d^2_j \; ; \; j=1,..,L$$

In the case under concern, we have $t = t_s$ and we may assume d_j = const. = h/2, so the rule for obtaining the coefficient of the matrix **D**, Eq. (4) is self-evident.

APPENDIX II

Let us consider Eq. (11) of the main text, where W is defined by (3). Furthermore we use Eq. (13) by assuming that the components of the vector $\mathbf{N}_{0max}$ are known functions of (x,y), and denote them, for sake of simplicity, by n_x, n_y, n_{xy}. Thus we have for the work associated with the membrane components:

$$\Pi_{N0} = \Psi_0 \sum_m \sum_n \sum_r \sum_s q_{mn}\, q_{rs}\, G_{mn,rs};$$

$$m,r = 1,...,M_1 \; ; \; n,s = 1,...,M_2$$

where, recalling the assumed shape functions (4):

$$G_{m\,n,\,r\,s} = n_x(\partial F_{mn}/\partial x)\,(\partial F_{rs}/\partial x) + 2n_{xy}(\partial F_{mn}/\partial x)(\partial F_{rs}/\partial y) + n_y(\partial F_{mn}/\partial y)(\partial F_{rs}/\partial y)$$

A suitable subscript condensation is necessary at this point. Thus we must define two indexes:

$$m_1 = (n-1)\, M_1 + m$$
$$m_2 = (r-1)\, M_1 + s$$

and, thus, we may re-write $G_{m\,n,\,r\,s}$ as $G_{m_1\,m_2}$.

By integrating the expression of $G_{m_1\,m_2}$ all over the wing area we obtain the coefficient (m_1,m_2) of the matrix $\mathbf{K}_{N0}$ of (14).

By the same procedure, by denoting the components of $\mathbf{N}_{1,max}$ as ν_x , ν_y, ν_{xy}, we obtain the components of the vector $\mathbf{R}_{N1}$ as the integral over the surface of the quantities:

$$r_{m_1} = \nu_x\,(\partial^2 F_{mn}/\partial x^2) \; + 2\,\nu_{xy}\,(\partial^2 F_{mn}/\partial x\,\partial y) + \nu_y(\partial^2 F_{mn}/\partial y^2)$$

again by using the above rule for subscripts condensation.

APPENDIX III

Active fibers are plastically deformed (generally, via axial elongation strain) and imbedded into a matrix (e.g. epoxy), in such a way that they cannot come back to the initial condition. When heated (via Joule effect), the fibers tend to come back to the condition previous to their deformation, but they are prevented to do that by the matrix.

As a consequence forces will arise in the plane of the sheet (and of the lamina), which are referred to as "recovery forces".

In order to compute this forces appearing in Eqs. (5) (6) one must known the field of the stresses arising in the active fibers, say σ_r^*; then, if V_α is the percent of active fibers, and T is the rotation matrix relevant to the theory of lamination [11], we w ill have:

$$[\sigma_x^*,\sigma_y^*,\sigma_{xy}^*] = T^{-1}\,[V_\alpha \sigma_r^*,0,0]$$

APPENDIX IV

In order to calculate the expression (23), let us firstly define the vector $\mathbf{Z}(x,y)$ of the describing functions (4), ordered as said in App. II, and the vector $\mathbf{H}(x,y)$ of the functions appearing in Eq. (17):

$$\mathbf{H}(m,n) = 1/c(y)\,\sqrt{[(1-u)/u]}\;u^n \sin[(2m+1)\,\theta]$$

Thus we may write :

$$C(x,y) = (\mathbf{J}_0 - \mathbf{J}_q)^T\,(\mathbf{A}^{-1})^T\,\mathbf{H}$$

and finally :

$$\int_\Sigma Cp(x,y)w(x,y)d\Sigma = (\mathbf{J}_0 - \mathbf{J}_q)^T\,(\mathbf{A}^{-1})^T\,\mathbf{M}\,\mathbf{q}$$

where :

$$\mathbf{M} = \int_\Sigma \mathbf{H}\,\mathbf{Z}^T\,d\Sigma$$

In the foregoing expression T denotes transpose of a vector or a matrix. From the above expression, one as clearly:

$$\mathbf{R}_0 = \mathbf{J}_0^T\,(\mathbf{A}^{-1})^T\,\mathbf{M}$$

$$\mathbf{R}_q = -\,\mathbf{J}_q^T\,(\mathbf{A}^{-1})^T\,\mathbf{M}$$

References

[1] J. Onada, T. Endo, H. Tamaoki, N. Watanabet, "Vibration Suppression by Variables-Stiffness Members", AIAA Journal, Vol. 29, No. 6, June 1991, pp 977-983.

[2] T. Bailey, J. E. Hubbard, "Distribuited Piezoelectric-Polymer Active Vibration Control of a Cantilever Beam", Journal of Guidance, Vol 8 No 5, pp 605-661.

[3] B. J. Maclean, G. J. Patterson, M. S. Misra, "Modeling of a Shape Memory Integrated Actuator for Vibration Control of Large Space Structure", Journal of Intelligence Material,Systems and Structures, Vol 2 Jan. 1991, pp 72-94.

[4] K. B. Lazarus, E. F. Crawley, J. D. Bohlmann, "Static Aerolastic Control Using Strain Actuated Adaptive Structures", Proceedings, First Joint U.S./Japan Conference on Adaptative Structure, Technomic, Lancaster, 1991.

[5] E. F. Crawley, K. B. Lazarus, "Induced Strain Actuation of Isotropic and Anisotropic Plates", AIAA Journal, Vol. 29, No. 6, June 1991, pp 944-951.

[6] C. Liang, J. Jia, C. A. Rogers, "Behavior of Shape Memory Alloy reinforced composite plates, Part I: Formulations and Conceps", Proceedings of the 30th Strctures, Structural Dynamics and Material Conference, Mobile, April 1989, pp 2011-2017.

[7] G. L. Giles, "Equivalent Plate Analysis of Aircraft Wing Box Structure with general Planform Geometry", Journal of Guidance, Vol. 23, No. 11, Nov. 1986, pp 859-864.

[8] J. W. Purvis, J. E. Burkhalter, "Simplified Solution of the Compressible Lifting Surface Problem", AIAA Journal, May 1982, pp 589-597.

[9] F. Persiani, G. M. Saggiani, "Modellazione Parametrica di Ali in Composito con Controllo Attivo delle Proprietà' del Materiale Mediante Calcolo Simbolico", XI congersso AIDAA Forlì 14-18 ottobre 1991.

[10] P. Santini, P. Gasbarri, "Aeroelasticita` statica dell'ala a freccia in materiale anisotropo", Atti del Dipartimento Aerospaziale 1991, Universita` la "Sapienza" Roma.

[11] P. Santini, "Costruzioni Aeronautiche", Esa, Milano, 1990.

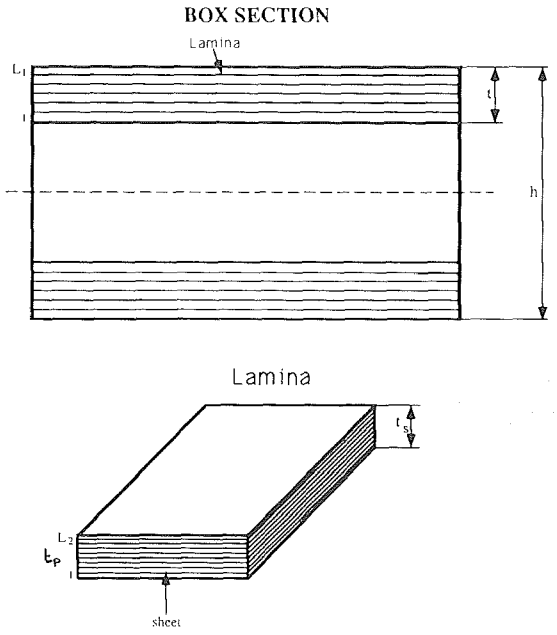

FIG. 1: SECTION GEOMETRY

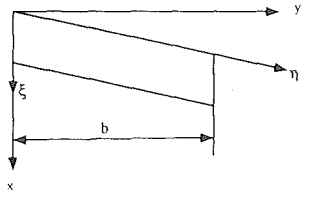

FIG. 2: Definition of rectangular and local coordinate

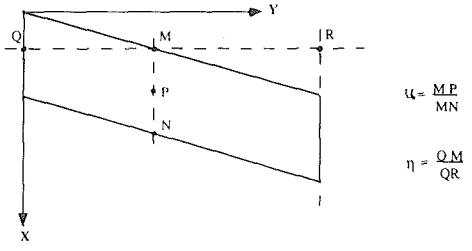

FIG. 3: Definition of coordinates

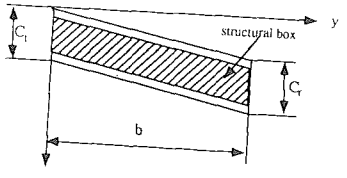

FIG. 4: Definition of lifting surface and of structural box

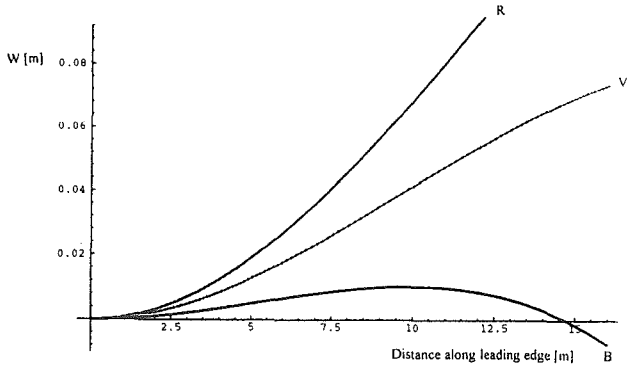

Fig . 5 : Elastic dispalcement along leading edge unswept wing:

R -> $\Psi_0 = \Psi_1 = 0$
V -> $\Psi_0 = \Psi_1 = 100$ MPa $\Lambda = 0$
B -> $\Psi_0 = \Psi_1 = 300$ MPa

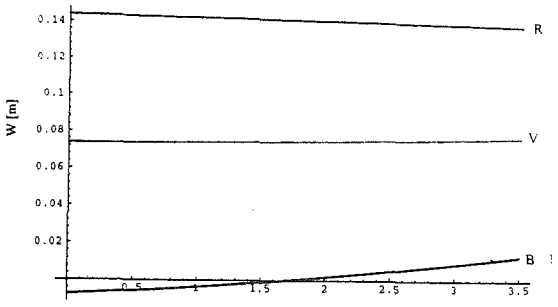

Fig . 6 : Distance along tip chord [m], same conditions as Fig. 5

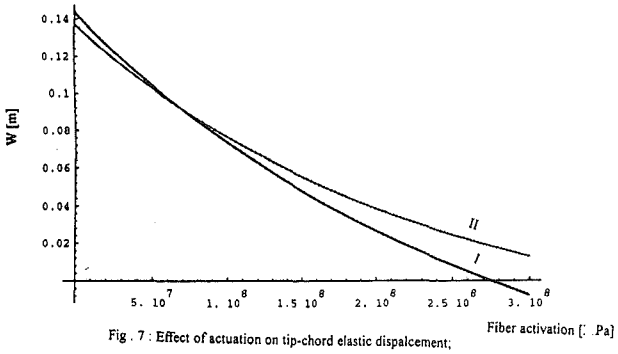

Fig . 7 : Effect of actuation on tip-chord elastic dispalcement;

I -> leading edge
II-> trailing edge

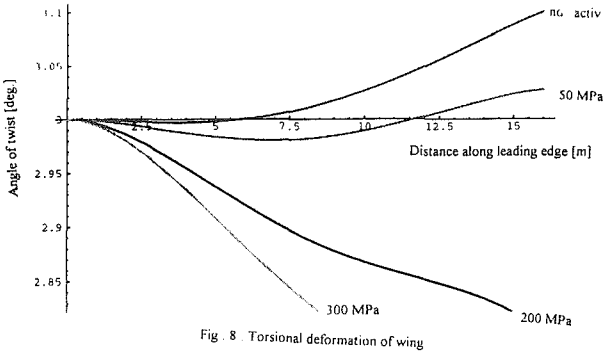

Fig . 8 : Torsional deformation of wing

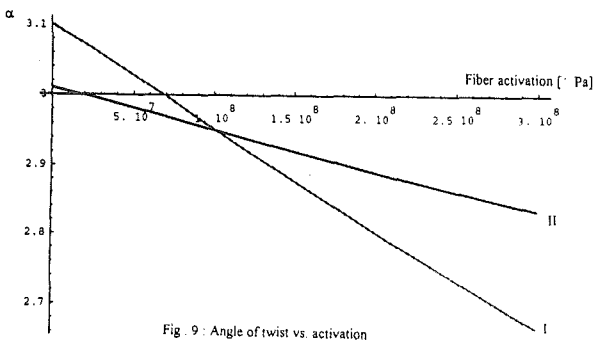

Fig . 9 : Angle of twist vs. activation

I -> wing tip
II -> wing half semispan

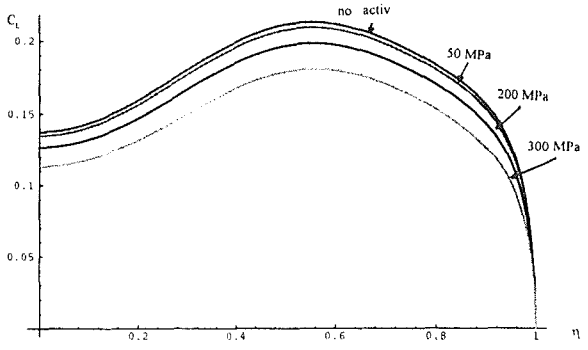

Fig 10 : Spanwise distribution of lift

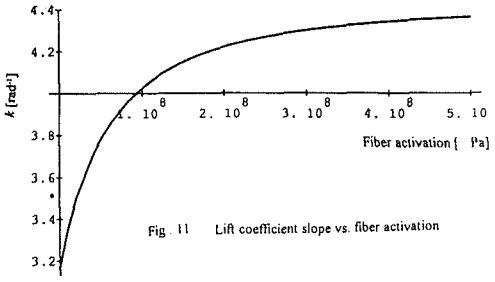

Fig . 11 Lift coefficient slope vs. fiber activation

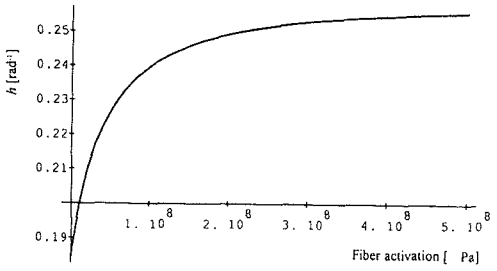

Fig . 12 Moment coefficient vs. fiber activation

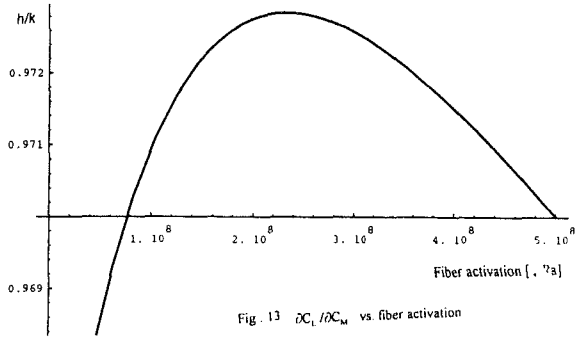

Fig . 13 $\partial C_L / \partial C_M$ vs. fiber activation

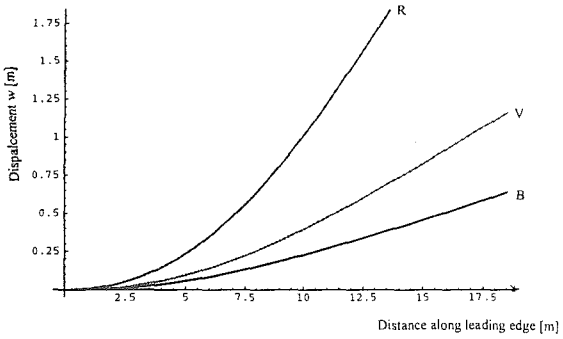

Fig . 14 : Elastic dispalcement along leading edge 30° backward swept wing

R -> $\Psi_0 = \Psi_i \approx 0$
V -> $\Psi_0 = \Psi_i \approx 100$ MPa
B -> $\Psi_0 = \Psi_i \approx 300$ MPa

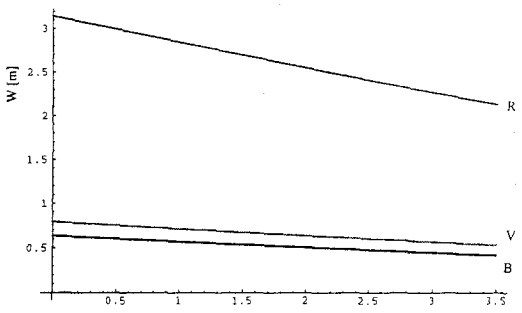

Fig . 15 : Distance along tip chord [m], same conditions as Fig. 14

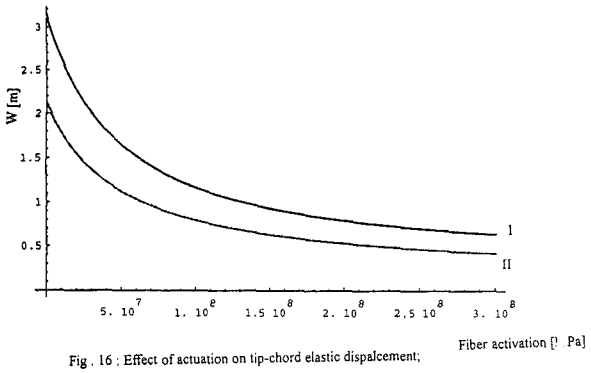

Fig . 16 : Effect of actuation on tip-chord elastic dispalcement;

I -> leading edge
II-> trailing edge

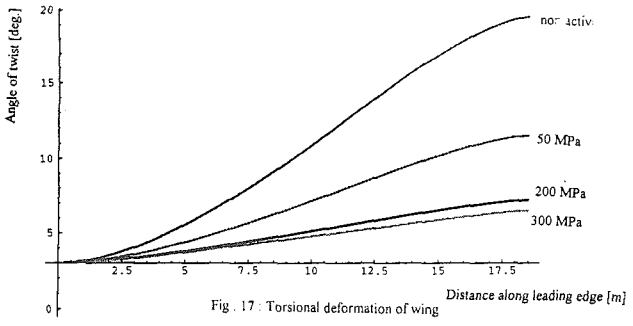

Fig . 17 : Torsional deformation of wing

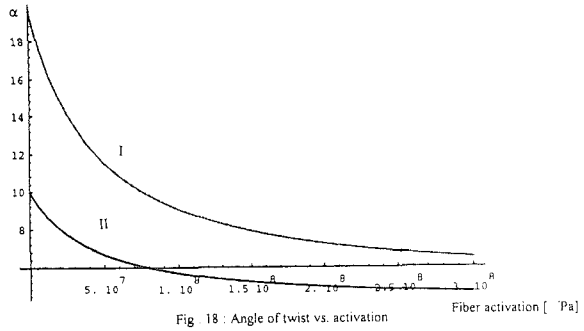

Fig 18 : Angle of twist vs. activation

I -> wing tip
II -> wing half semispan

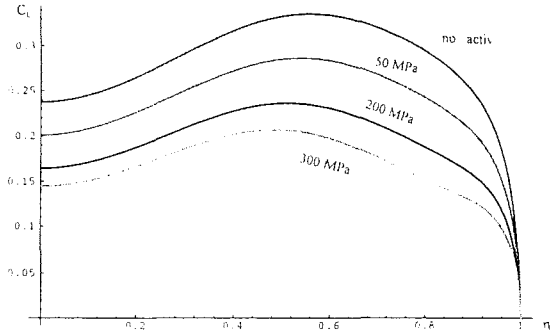

Fig 19 Spanwise distribution of lift

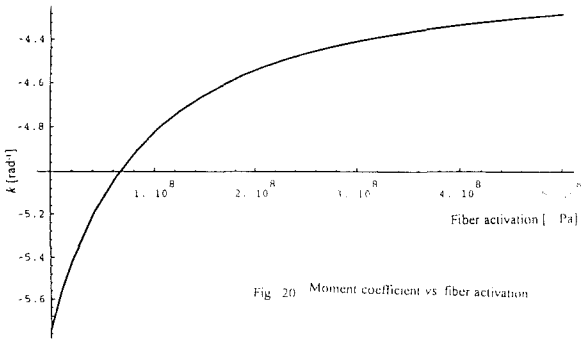

Fig 20 Moment coefficient vs fiber activation

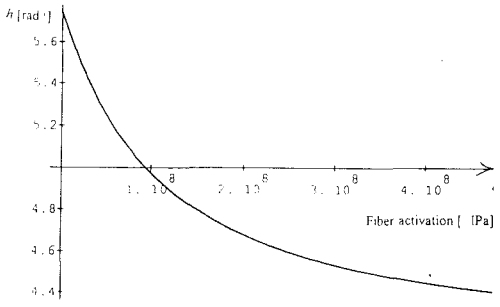

Fig 21 Lift coefficient slope vs fiber activation

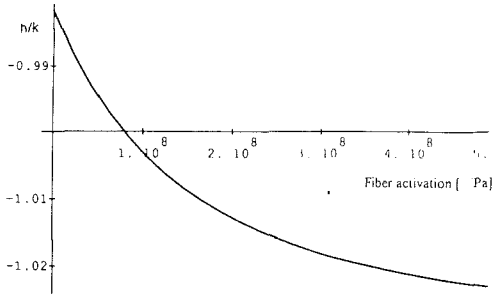

Fig 22 $\partial C_l / \partial C_M$ vs fiber activation

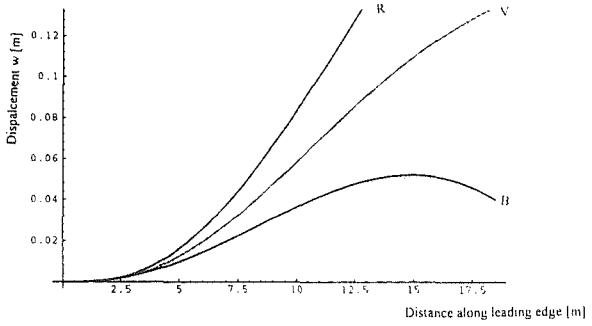

Fig. 23 Elastic dispalcement along leading edge 30° forward swept wing

R -> $\Psi_0 = \Psi_1 = 0$
V -> $\Psi_0 = \Psi_1 = 100$ MPa $\quad \Lambda = +30°$
B -> $\Psi_0 = \Psi_1 = 300$ MPa

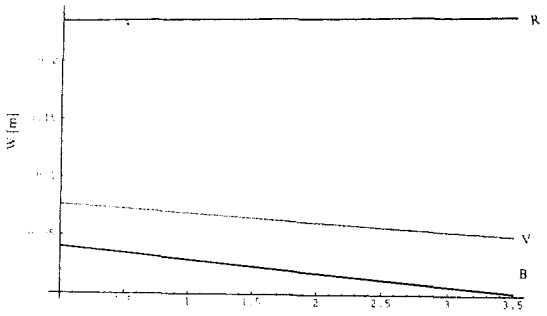

Fig. 24 Distance along tip chord [m], same conditions as Fig. 23

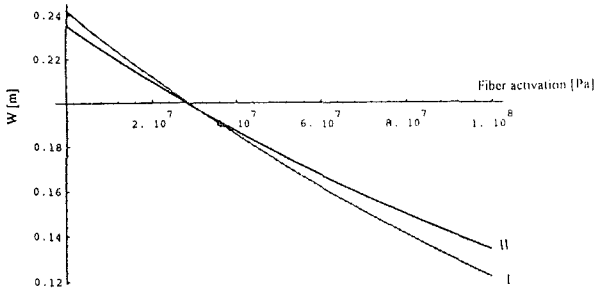

Fig. 25 Effect of actuation on tip-chord elastic dispalcement.

I -> leading edge
II-> trailing edge

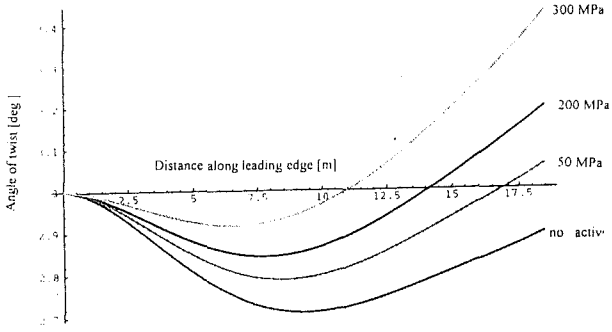

Fig. 26 Torsional deformation of wing

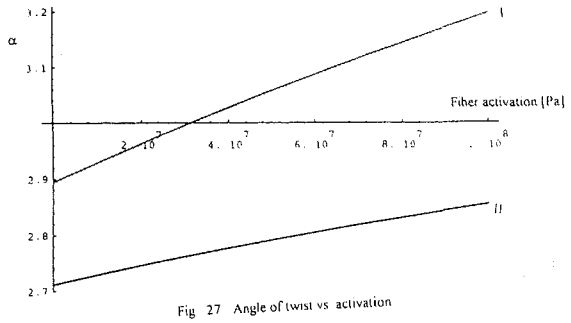

Fig 27 Angle of twist vs activation

I -> wing tip
II -> wing half semispan

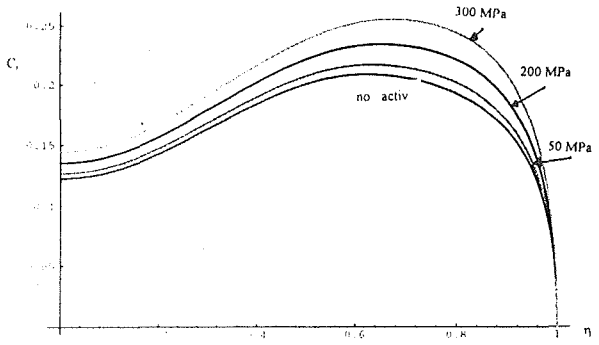

Fig 28 Spanwise distribution of lift

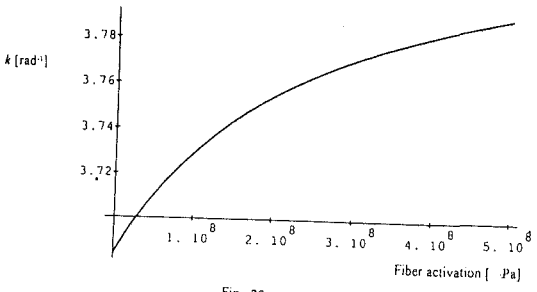

Fig 29 Lift coefficient slope vs fiber activation

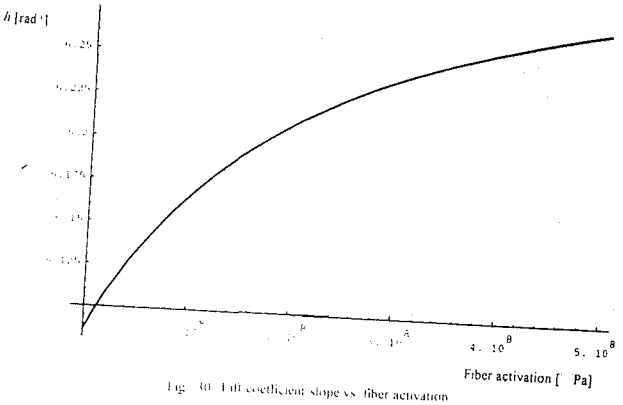

Fig 30 Lift coefficient slope vs fiber activation

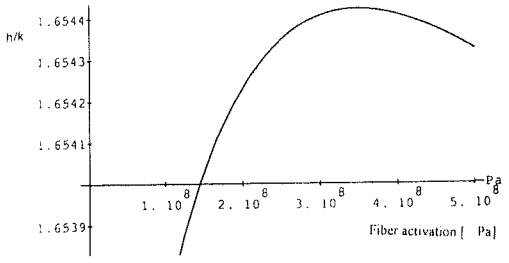

Fig 31 $\partial C_l / \partial C_{l_0}$ vs fiber activation